2026 IEEE International Conference on Robotics and Automation (ICRA 2026)
June 1-5, 2026. Vienna, Austria

A Multisensory Neurofeedback–Based Immersive BCI Paradigm for Emotion Regulation

Lianchi Zhang†, Bowen Fu†, Jingting Zhang*, Shoucheng Yang, Zonghai Huang, Rui Huang, and Hong Cheng

***Abstract*—Enhancing brain activation efficiency is crucial in developing brain computer interface (BCI) paradigm for cognitive rehabilitation. However, the existing BCI paradigms mostly achieved limited sensory-activation without sufficient feedback of mind and body, significantly limiting the user engagement and training efficiency. In this study, we propose a novel multisensory neurofeedback framework to develop an immersive BCI paradigm for emotion regulation, supported by a novel panoramic motion-based virtual reality system. The paradigm is designed to promote deeper cognitive and physical involvement in functional brain training. It delivers multisensory neurofeedback—visual, auditory, and motor—through the Gait Real-time Analysis Interactive Lab system and incorporates cognitive reappraisal from the modified Gross procedure for emotion regulation. Its effectiveness is validated through three experimental studies, including event-related potential analysis, power spectral density analysis, and brain network analysis. The results demonstrate that the paradigm enhances motor–cognitive interaction and multisensory coordination, effectively increasing brain activation in visual, auditory, and motor processing regions, and further promoting stronger engagement of emotion regulation-related areas such as the prefrontal cortex. Compared with conventional paradigms, the proposed paradigm increases the number of high-intensity functional connections by 28.6% (from 42 to 54) and the number of effective functional connections by 42.3% (from 71 to 101).**

I. Introduction

Closed-loop brain training is an important technology for motor and cognitive rehabilitation, which has received ever-increasing attention in the field of Brain Computer Interface (BCI) [1]. The design of BCI paradigms plays a pivotal role in advancing closed-loop rehabilitation and brain training, and has drawn growing attention in recent research. For instance, Nguyen et al. [2] developed a paradigm based on the International Affective Picture System (IAPS) for brain imaging studies related to emotion processing and regulation. They successfully identified detailed causal brain networks associated with this function and investigated network changes that facilitate different emotional states.. Similarly, Li et al. [3] developed an experimental paradigm based on the IAPS to investigate the effects of transcranial magnetic stimulation applied to different brain regions on the cognitive reappraisal function, and identified the impacts of different emotions on brain region activation within the emotion regulation network. Despite these advances, most of existing BCI paradigms achieved limited sensory-activation without sufficient feedback of mind and body, limiting their capability of effectively activate and coordinate the targeted brain functional regions during training tasks. [4].

Neurofeedback has been recognized as a potentially effective technique to enhance both user engagement and training efficiency in BCI paradigms. It operates by continuously monitoring neural activity in real time, adjusting training parameters according to predefined strategies, and providing sensory feedback that enables participants to modulate their own brain states. Several studies have explored the application of neurofeedback in BCI. For example, Watve et al. [5] applied real-time fMRI neurofeedback with naturalistic facial displays as visual feedback to guide participants' regulation of emotion-related brain regions. Pereira et al. [6] implemented a thermometer-like bar display updated every two seconds to provide visual feedback in clinical neurofeedback training, successfully improved users' regulation of specific neural oscillations. However, most existing methods have focused on unimodal feedback, without achieving integrated multisensory feedback and regulation. As a result, they fall short in ensuring comprehensive mental and physical engagement during training tasks, which is critical for the effectiveness of cognitive rehabilitation [7].

In this study, we propose a novel multisensory neurofeedback framework to develop an immersive BCI paradigm for emotion regulation, implemented through a motion–panoramic virtual reality (VR) system. The paradigm builds on the Gross model [8] and is realized using the Gait Real-time Analysis Interactive Lab (GRAIL) platform. The system can remarkably provide a multisensory feedback training, including wide-angle visual feedback, multichannel auditory feedback, and motion platform feedback. This indeed establishes a panoramic immersive environment to significantly enhance task engagement and improve the overall user experience [9]. To evaluate the effectiveness of

Lianchi Zhang, Bowen Fu, Jingting Zhang, Shoucheng Yang, Zonghai Huang, Rui Huang, and Hong Cheng are with the Center for Robotics, School of Automation Engineering, University of Electronic Science and Technology of China, Chengdu 611731, China. *Jingting Zhang is the corresponding author (e-mail: zhangjt@uestc.edu.cn).

This work was supported in part by the National Natural Science Foundation of China (Grant 62403104, 62473079), the Natural Science Foundation of Sichuan Province (Grant 2025ZNSFSC1518), the Fundamental Research Funds for the Central Universities (Grant ZYGX2024XJ028, ZYGX2025YGLH005), the Foundation of Nursing Key Laboratory of Sichuan Province (Grant No. HLKF2024(Z)-3). †Lianchi Zhang and Bowen Fu contribute equally to this paper.

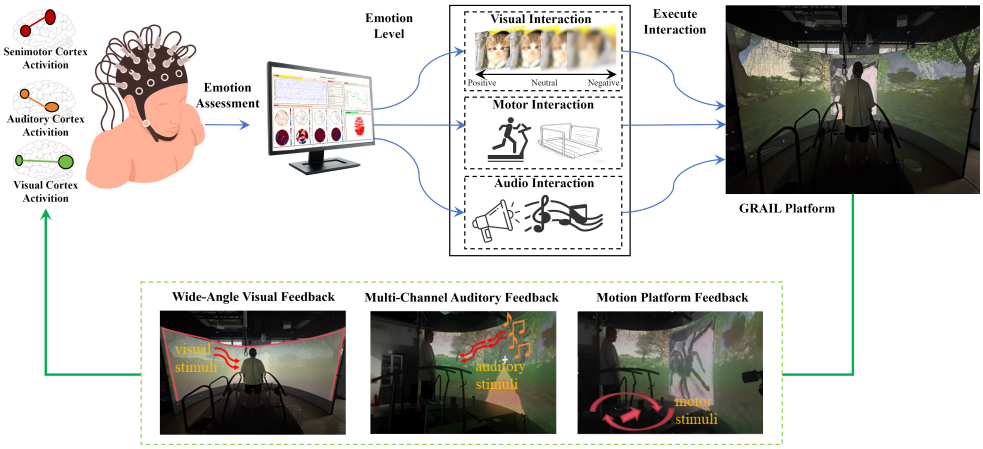

Fig. 1: Overview of the proposed multisensory neurofeedback-based immersive BCI paradigm with the GRAIL platform.

the proposed paradigm, electroencephalogram (EEG) data were collected from five participants across three experimental protocols, including event-related potential (ERP) analysis, power spectral density (PSD) analysis, and brain network analysis. A conventional computer-based paradigm was also introduced as a baseline for comparison with the GRAIL-based immersive paradigm. The experimental results demonstrate that the proposed paradigm exhibits superior performance in motor–cognitive interaction and multisensory integration. This improvement can be attributed to the synchronized multisensory feedback mechanism involving visual target perception, auditory conflict suppression, and motor execution. Further analyses reveal that this mechanism not only enhances neural activation in the visual, auditory, and motor cortices, but also more effectively recruits brain regions associated with emotion regulation, such as the prefrontal cortex.

The main contributions of this study are summarized as follows: 1) We present, for the first time, an immersive BCI paradigm developed on the GRAIL platform that leverages motion–panoramic VR technology. This design enables profound mental and physical engagement of participants within the task, thereby ensuring the intended level of involvement in BCI training; 2) The proposed paradigm integrates multisensory neurofeedback across visual, auditory, and motor modalities, which effectively stimulates multiple sensory-related cortical regions and, through the integration of multimodal feedback, enhances the activation of brain areas associated with emotion regulation.

II. Methods

A. Immersive BCI Paradigm for Emotion Regulation

As seen in Fig.1, our BCI paradigm is developed with a novel multi-sensory neurofeedback framework and supported by the GRAIL platform. This paradigm is designed for emotion regulation, as an example to facilitate subsequent introduction. The paradigm is designed to secure profound mental and physical engagement of participants during brain training tasks related to emotion regulation. By integrating visual feedback elements, auditory feedback via music, and proprioceptive feedback from leg movements, it simultaneously delivers visual, auditory, and motor stimulation.

The experimental procedure is inspired by the Gross model of emotion regulation, with particular emphasis on adapting the cognitive reappraisal component. Participants were required to complete tasks in a virtual forest trail environment. At the beginning of each trial, a cue appeared on the screen specifying the type of task to be performed, which included two conditions: free viewing and reappraisal. Following the cue, an image designed to elicit a particular emotional state (positive, neutral, or negative) was displayed in GRAIL, and participants were instructed to regulate their emotions according to the given task requirements.

Specifically, in the reappraisal trials, participants combined walking and neurofeedback to assist in the completion of immersive emotion regulation, as shown in Fig. 2. During the implementation of emotion regulation, the EEG characteristics (alpha/beta bands) of the participants are continuously extracted as indicators of the negative emotion intensity and transmitted to the interactive paradigm. Specifically, the higher the negative emotion intensity index, the lower the clarity of the visual stimulus elements presented by the paradigm, the lower the volume of the music used as the auditory stimulus, and the faster the speed of the platform that assists the participants in walking. By providing neurofeedback of EEG indices in the form of multimodal sensory stimulus parameters, the paradigm enables participants to reduce their exposure to emotion-inducing sources when experiencing high levels of negative emotions, and to inhibit negative emotions through movement—ultimately allowing them to complete the emotion regulation process in a more intuitive manner.

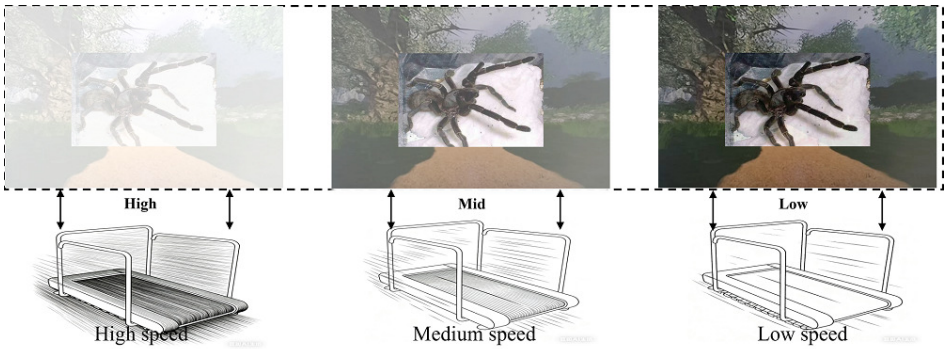

Fig. 2: The implementation mode of neurofeedback in the immersive paradigm corresponds to the levels of negative emotion from high to low from left to right.

B. Multisensory Neurofeedback Framework for Brain Network Activation

The proposed multisensory neurofeedback framework integrates visual, auditory and motor in conjunction with the GRAIL system, as seen in Fig. 1. This integration facilitates coordinated regulation of motor–cognitive interaction and multimodal feedback, thereby enhancing neural activation within the visual cortex, auditory cortex, and motor-related cortical regions. Moreover, multisensory neurofeedback is capable of modulating oscillatory dynamics in the prefrontal–limbic circuitry as well as the thalamo–cortical loops, which enables cross-modal information integration and fosters synergistic activation of emotion regulation–related brain regions such as the prefrontal cortex and cingulate cortex [10], [11]. These mechanisms will be further examined in subsequent brain network analyses.

1) ***Wide-Angle Visual Feedback****:* The visual feedback module is built upon the wide-angle visual rendering system of GRAIL, which projects dynamic forest-walking scenarios onto a 180° immersive curved screen to deliver visual stimulation. The system consists of multiple visual layers: (i) Environmental layer: continuous mountain ranges and dense woodlands forming the geographical boundaries; (ii) Interactive layer: rendered by a real-time physics engine, generating a trail that dynamically synchronizes with the participant's movements. On this basis, during the cognitive reappraisal stage of the paradigm, emotional images presented at the center of the screen are partially obscured by a fog overlay, the intensity of which is mapped to the participant's negative emotion index. This mechanism enables participants to visualize the regulation of their own emotional states during reappraisal. The module effectively activates visual cortical regions and, through neurofeedback, encourages participants in negative states to concentrate more on the cognitive reappraisal task itself, thereby enhancing task engagement.

2) ***Multi-Channel Auditory Feedback****:* The auditory feedback module is implemented through GRAIL's multi-source sound system, ensuring synchronization of auditory effects with visual scenes. In addition to the environmental background sounds embedded in the paradigm, when emotional images are displayed by the visual feedback module, the system plays music that matches the same emotional category, thus providing auditory stimulation. The music is selected along two dimensions—arousal and valence—to maximize the induction of target emotional states. During the cognitive reappraisal stage, the loudness of the music is dynamically coupled with the fog overlay effect: under conditions of high negative emotion, the volume is attenuated, and as participants successfully regulate their negative emotions, the loudness gradually returns to normal, completing the adaptive reappraisal process. By incorporating these synchronized elements, the module provides real-time auditory feedback during emotion regulation, not only strengthening participants' immersive experience but also enhancing task engagement and increasing activation of auditory cortical regions.

3) ***Motion Platform Feedback****:* The embodied feedback module employs a walking motion platform, enabling the delivery of somatic stimulation during the cognitive reappraisal stage. Its mechanism relies on the backward operation of the treadmill integrated within the GRAIL system, allowing participants to walk naturally while performing the task. During emotion regulation, moderate motor assistance helps mitigate negative affect. In addition to the visual and auditory feedback mapped to indices of negative emotion, the motion feedback provided by the GRAIL platform further supports participants in effectively completing reappraisal tasks and alleviating the influence of negative states. As participants gain control over their negative emotions, the treadmill speed progressively decreases from fast to slow, mirroring the gradual transition from heightened arousal to calmness. Working in concert with the other sensory feedback modules, this component not only recreates a psychologically valid immersive context for emotion regulation but also enhances activation of the sensorimotor cortex and promotes coordinated engagement of the cognitive–motor neural network.

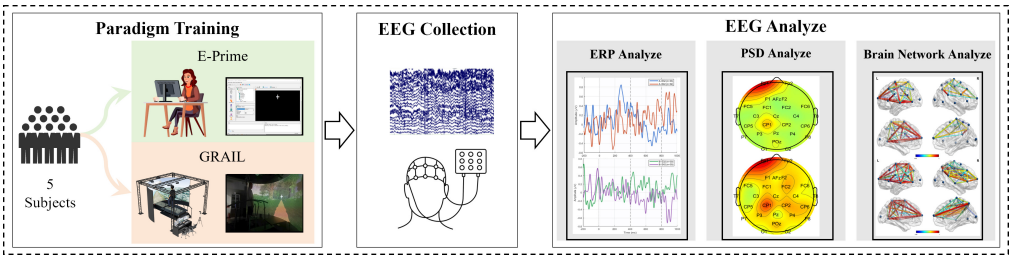

Fig. 3: The experimental workflow used to validate the effectiveness of the proposed paradigm.

C. Participants and Experimental Setup

Five healthy participants took part in this study (5 males; aged 19-23 years), and the experimental procedure is depicted in Fig. 3. EEG signals were recorded using a 32-channel acquisition system configured according to the international 10–20 electrode placement standard. To examine the effects of the proposed multisensory neurofeedback immersive paradigm (hereafter referred to as the immersive paradigm) on brain activation, we also implemented a conventional emotion regulation paradigm consistent with the Gross protocol (hereafter referred to as the standard paradigm) on a computer platform. While the standard paradigm retained the emotion induction and cognitive reappraisal components, it excluded the motor and auditory modules. In this setup, stimuli were presented as colored images against a white background. Under both paradigms, participants completed four instructed conditions: free viewing of positive, neutral, and negative images, as well as cognitive reappraisal. Each experiment comprised 40 trials.

ERP analysis was first conducted to determine whether the immersive paradigm could elicit distinct neural responses in emotion regulation–related regions during the reappraisal phase. PSD analysis was then applied to quantify activation levels in the visual, auditory, and motor cortices, along with regions implicated in emotion regulation (particularly the prefrontal cortex, PFC). Finally, brain network analysis was performed to compute functional connectivity metrics across cortical regions, allowing us to assess the influence of the immersive paradigm, when employed as an NFT task, on overall brain functional connectivity. By comparing these neural indices and activation differences between paradigms, we aimed to characterize interregional coordination patterns and further validate the feedback training effect of the immersive paradigm on emotion regulation.

D. EEG Data Preprocessing

The acquired 32-channel EEG signals were first re-referenced using a whole-brain average, then downsampled to 250 Hz, and subsequently band-pass filtered between 1–30 Hz to suppress noise. Epochs were segmented with the onset of the cognitive reappraisal cue serving as time zero, and multiple time windows were extracted for analysis. Trials of the same event type across different sessions were then averaged to improve signal reliability [12]. For subsequent analyses, visual cortical activity was assessed using data from electrodes O1, O2, Oz, POz, P7, and P8; auditory cortical responses were examined from electrodes T7 and T8; motor-related activity was analyzed through electrodes C3, C4, Cz, FC1, FC2, FC5, and FC6; and emotion regulation–related regions were evaluated using electrodes CP1, CP2, Pz, and Cz [13].

E. Event-Related Potential Analysis

The Late Positive Potential (LPP) typically emerges within 400–800 ms after stimulus onset and can persist up to 1000 ms, serving as a crucial ERP index for emotional processing and regulation. In the paradigm of the present study, we focus on examining the LPP amplitudes elicited by emotional picture stimuli (negative, neutral, positive) under different regulatory conditions (e.g., passive viewing and reappraisal). A typical characteristic of the LPP is a sustained positive deflection in the central-parietal regions (e.g., Cz, CP1, CP2, Pz), which reflects enhanced allocation of attention and motivational resources by individuals toward emotionally salient stimuli [14].

Following the allocation protocol, EEG data within the time window of $[-200, 1000]$ ms were analyzed, with the pre-stimulus interval from -200 to 0 ms used for baseline correction. By comparing LPP amplitudes across different emotional categories and regulatory conditions, we tested whether reappraisal could reduce the LPP response to negative stimuli, thereby reflecting the successful downregulation of emotional responses.

F. Power Spectral Density Analysis

To assess the activation strength of visual, auditory, motor, and emotion regulation–related brain regions, PSD was estimated using Welch's method. For each EEG channel, the analysis window was defined as a 1-second interval immediately following the onset of the cognitive reappraisal task. Within this window, the mean spectral power was computed across the 1–30 Hz frequency range, with sub-bands of interest including δ (1–4 Hz), θ (4–8 Hz), α (8–12 Hz), and β (12–30 Hz).

The PSD for electrode p, frequency bin f_q, and region s, written as $P_{p,f_q,s}$, is defined as:

$$P_{c,f_k,r} = \frac{1}{KMU} \sum_{m=1}^{K} \left| \sum_{n=0}^{M} x_{i,c}[n] w[n] e^{-u 2\pi k n / M} \right|^2 \quad (1)$$

where $x_{i,c}[n]$ denotes the $(n+1)$-th sampled value within the m-th segment of channel c; $w[n]$ represents a tapering function of size M; M indicates the segment duration in samples; K is the total number of divided segments; U corresponds to the normalization constant of the window; u denotes the imaginary unit; and $f_k = k \cdot f_s/M$ specifies the frequency associated with index k, with f_s being the sampling rate. Here, k identifies the discrete spectral bin within the frequency domain.

G. Brain Network Analysis

Next, we examine how the activity of participants' visual, auditory, and motor cortices contributes to the modulation of emotion regulation networks. In line with the approach of [15], functional connectivity between channel X and channel Y is quantified using the Pearson correlation coefficient (r_{XY}), as defined in (2), which captures the temporal co-variation of their signals:

$$r_{XY} = \frac{\sum_{n=1}^{M_c}(X_n - \bar{X})(Y_n - \bar{Y})}{\sqrt{\sum_{n=1}^{M_c}(X_n - \bar{X})^2 \sum_{n=1}^{M_c}(Y_n - \bar{Y})^2}} \tag{2}$$

Here, X_n and Y_n denote the voltage values of channels X and Y at the n-th sampling point, while $\bar{X}$ and $\bar{Y}$ represent their respective mean values. M_c is the total number of samples considered. The Pearson correlation coefficient reflects the degree of linear association between two signals, with values ranging from –1 to +1, where positive values indicate direct coupling, negative values indicate inverse coupling, and values near zero imply little to no linear dependency.

After calculating the Pearson correlation coefficient between each pair of electrodes (excluding mastoid reference electrodes M1 and M2), the 30×30 weighted adjacency (connectivity) matrix is achieved to denote interactions among the 30 nodes for each averaged trial. Then, the brain network is constructed based on the 30×30 weighted adjacency (connectivity) matrix using the corresponding Pearson correlation coefficient as the network edge between nodes i and j, where r_{ij} represents the edge linkage strength between nodes i and j obtained by Eq. 2. To facilitate a more intuitive comparison of functional connectivity patterns across brain regions, the functional connectivity matrices are visualized using the BrainNet Viewer toolbox in MATLAB [16].

In addition to examining functional connectivity matrices, we further describe network properties by computing a set of graph-theoretical measures. Specifically, we evaluate the Phase Locking Value (PLV in (3)), which captures the degree of phase synchronization between neural signals; local efficiency (L_e in (4)), which reflects the robustness of information exchange when individual nodes are removed; the mean node degree ($\langle d \rangle$ in (5)), which characterizes the overall level of connectivity across the graph; and the characteristic path length (L in (6)), which measures the average efficiency of information transmission through the network. The formal definitions of these metrics are given below:

$$PLV = \frac{1}{M_c}\left|\sum_{n=1}^{M_c} e^{u(\phi_i(n)-\phi_j(n))}\right| \tag{3}$$

$$L_e = \frac{1}{N}\sum_{i=1}^{N}\frac{\left(\sum_{j,h\in C_i,\ j\neq h} l_{hj}^{-1}\right)}{(N_i(N_i-1))} \tag{4}$$

$$\langle d \rangle = \frac{1}{N}\sum_{i=1}^{N} d_i \tag{5}$$

$$L = \frac{1}{N}\sum_{i\in C}\frac{\sum_{j\in C, j\neq i} l_{ij}}{(N-1)} \tag{6}$$

where $\phi_i(n)$ and $\phi_j(n)$ denote the instantaneous phases of nodes i and j at time n; u is the imaginary unit; N is the total number of nodes; C represents the set of all nodes; C_i is the set of neighbors of node i; N_i is the number of neighbors of node i; l_{ij} is the shortest weighted path length between nodes i and j; and d_i indicates the degree, i.e., the number of edges connected to node i.

Together, these complementary indices provide a more complete description of the brain network's topological structure and its functional integration.

III. Experimental Results

A. ERP Analysis Results

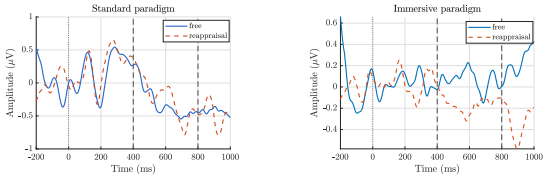

(a) LPP amplitude changes in the standard paradigm.

(b) LPP amplitude changes in the immersive paradigm.

Fig. 4: Comparative LPP amplitude changes observed in the emotion regulation under immersive and standard paradigms.

For the EEG data recorded at the central-parietal electrodes (CP1/CP2), trials under the two conditions (free viewing and reappraisal) were averaged, and the grand-averaged waveforms are presented in Fig. 4. Consistent with previous studies, a significant LPP was observed in both conditions within the 400–800 ms time window after stimulus onset.

In the standard paradigm, both conditions elicited distinct LPP responses. Compared with free viewing, the LPP amplitude under the reappraisal condition was slightly lower in the later phase, and this difference persisted within the 400–800 ms time window. The amplitude of EEG signals during the emotion regulation phase within this time window is reduced by approximately 0.05 μV on average compared to that during the emotion induction phase. This suggests that reappraisal in Group A could slightly reduce individuals'

responses to emotional stimuli, which is consistent with findings in existing literature.

In the immersive paradigm, both conditions also induced sustained LPPs; however, the LPP amplitude under the reappraisal condition was significantly lower than that under free viewing. The amplitude of EEG signals during the emotion regulation phase within this time window is reduced by approximately 0.2 μV on average compared to that during the emotion induction phase. This reduction reflects a more successful downregulation effect, indicating that the immersive paradigm effectively decreases individuals' emotional engagement with emotional stimuli during reappraisal.

Comparison of the LPP signals elicited by the two paradigms reveals that the LPP exhibits differential regulatory effects across conditions: in the standard paradigm, reappraisal slightly reduced the LPP amplitude; in contrast, in the immersive paradigm, reappraisal led to a significant reduction in LPP amplitude. This finding confirms that the LPP is a sensitive and reliable neural index during emotion regulation, with prominent manifestations in the central-parietal brain regions. Additionally, when the same baseline is used for both paradigms, it is found that the immersive paradigm elicits a more pronounced LPP, which indicates that this paradigm can induce stronger emotional responses.

B. PSD Analysis Results

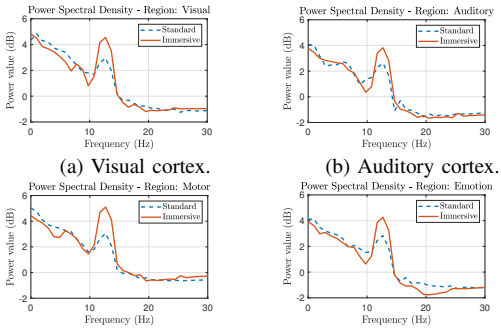

(a) Visual cortex. (b) Auditory cortex.

(c) Motor cortex. (d) Emotion cortex.

Fig. 5: Comparison of PSD of average trial EEG signals in four brain regions between immersive and standard paradigms.

To examine the differential effects of the immersive and standard paradigms on the activation of visual, auditory, motor, and emotion regulation-related brain regions, PSD analysis was applied to EEG signals from each region. For both paradigms, EEG data recorded during reappraisal trials were segmented into 2-second windows with 500 ms overlap, averaged across trials, and then used to compute PSDs for the electrodes corresponding to each brain region. Channel-wise PSDs were further averaged within regions to obtain the spectral distribution of EEG power across the 1–30 Hz range (Fig. 5). To assess differences in α-band suppression between the two paradigms, three 8-second epochs were

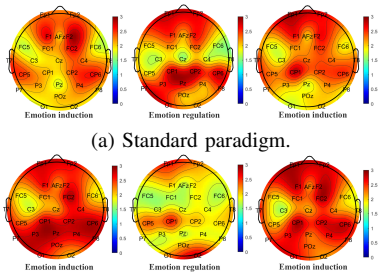

(a) Standard paradigm.

(b) Immersive paradigm.

Fig. 6: Comparison of alpha band power changes during emotion regulation in average trial EEG signals across all channels between immersive and standard paradigms. Blue indicates alpha suppression, meaning higher activation.

analyzed: during the reappraisal phase and during the free-viewing periods immediately before and after reappraisal. For each epoch, mean α power across channels was calculated, and topographic maps were generated to illustrate temporal changes (Fig. 6).

In the standard paradigm (Fig. 5(a)), PSD curves across the four brain regions followed a general trend of power decreasing with frequency, reaching a trough in the α band, increasing again in the lower β range, and then gradually declining. The temporal dynamics of α power revealed relatively modest changes, with suppression largely confined to parietal regions (Fig. 6(a)).

In contrast, the immersive paradigm (Fig. 5(b)) produced PSD curves with a similar overall shape, but differences emerged in the magnitude of α minima and β maxima. Temporally, the immersive design elicited robust α power fluctuations across nearly all channels around the reappraisal phase (Fig. 6(b)). Specifically, α power reductions in the occipital, parietal, and temporal regions indicated recruitment of the visual and auditory cortices; rapid α suppression in the PFC was linked to cognitive aspects of emotion regulation; and decreases in central regions reflected motor cortex activation during movement execution.

Comparison of PSD results showed that the immersive paradigm yielded lower α band power than the standard paradigm, indicating stronger α suppression. Concurrently, higher β power under the immersive condition suggested greater engagement of the four cortical systems. Topographic analyses of α power dynamics further revealed that the standard paradigm (limited to visual stimuli) primarily activated parietal areas with modest intensity changes, whereas the immersive neurofeedback paradigm induced broader and stronger activations across visual, auditory, motor, and emotion regulation networks, highlighting its superior capacity for multisensory neural stimulation.

C. Analysis Results of Brain Network Functional Connectivity

To assess the differences in functional brain activation and training efficacy between the two NFT game paradigms,

TABLE I: Network metrics for various functional brain regions on the standard paradigm and immersive paradigm

Subject	Metric	Emotion		Visual		Auditory		Motor	
		Standard	**Immersive**	Standard	Immersive	Standard	**Immersive**	Standard	**Immersive**
S01	Phase-Locking Value	0.3739	**0.4420**	0.6525	**0.7514**	0.3888	**0.5201**	0.5003	**0.5849**
	Node Degree(Mean)	1.7763	**1.8589**	3.9106	**4.1838**	0.2957	**0.6380**	3.0535	**3.1649**
	Local Efficiency	0.6905	**0.7886**	0.7834	**0.8368**		NaN	0.6817	**0.6640**
	Characteristic Path Length	1.8713	**1.2667**	1.3176	**1.2128**	1.7066	**1.5551**	2.4053	**2.2451**
S02	Phase-Locking Value	0.3236	**0.4037**	0.5420	0.5423	0.3107	**0.3003**	0.4906	**0.5293**
	Node Degree(Mean)	1.0070	**1.4722**	3.2025	**3.3033**	0.2963	**0.3819**	2.6732	**3.2656**
	Local Efficiency	0.7056	**0.7148**	0.7460	**0.7692**		NaN	0.6732	**0.7583**
	Characteristic Path Length	1.5168	**1.1392**	1.7253	**1.7104**	1.8636	**1.7478**	2.5752	**2.1731**
S03	Phase-Locking Value	0.4965	**0.4807**	0.4243	**0.5596**	0.3853	**0.5613**	0.5598	**0.6887**
	Node Degree(Mean)	2.4821	**2.5389**	1.9737	**2.7872**	0.2627	**0.5194**	3.7154	**3.7233**
	Local Efficiency	0.7363	**0.7766**	0.7174	**0.7332**		NaN	0.6626	**0.7194**
	Characteristic Path Length	2.3362	**2.2235**	2.3994	**1.9195**	1.6038	**1.2645**	1.9195	**1.9009**
S04	Phase-Locking Value	0.4831	**0.4763**	0.6988	**0.7545**	0.4418	**0.5105**	0.4917	**0.5484**
	Node Degree(Mean)	2.5233	**2.5953**	3.9866	**4.1209**	0.3684	**0.6025**	3.0574	**3.3417**
	Local Efficiency	0.7484	**0.7618**	0.8189	**0.8242**		NaN	0.6667	**0.6808**
	Characteristic Path Length	2.3357	**2.2912**	1.3440	**1.2384**	1.7170	**1.5642**	2.3824	**2.0011**
S05	Phase-Locking Value	0.4857	**0.5347**	0.7127	**0.7611**	0.5095	**0.5212**	0.5487	**0.5877**
	Node Degree(Mean)	2.4963	**2.5631**	4.0204	**4.1760**	0.4267	**0.6394**	3.1914	**3.5862**
	Local Efficiency	0.7406	**0.7513**	0.8057	**0.8352**		NaN	0.6611	**0.6920**
	Characteristic Path Length	2.3731	**2.2839**	1.2766	**1.2198**	1.5940	**1.5412**	2.1228	**1.9339**

Note: NaN values in the Auditory region indicate that calculation is not possible due to only having two channels.

this study calculated the average brain network measures (including PLV, local efficiency, mean node degree, and characteristic path length) across all cognitive reappraisal trials for each participant, thereby characterizing the overall level of functional activation. The corresponding results are presented in Table I.

As shown in the table, although inter-individual variability remains, most brain network metrics in the emotion regulation–related cortex, auditory cortex, visual cortex, and motor cortex exhibit higher values under the immersive paradigm compared to the standard paradigm. Notably, the immersive paradigm yields the most prominent improvements in mean node degree within the auditory cortex, PLV and local efficiency within the motor cortex, and characteristic path length within the emotion regulation–related cortex. Overall, when comparing the two paradigms, the results indicate that the immersive paradigm consistently achieves stronger and more stable activation in the emotion regulation–related and visual cortices, while also producing significant enhancements across all metrics in the auditory and motor cortices. These findings suggest that the multimodal sensory feedback provided by the immersive paradigm effectively strengthens functional activation in these brain regions.

To assess the training effects of the immersive paradigm, trials from all cognitive reappraisal events in both the initial and final experimental sessions were averaged for each participant. Brain network analysis was then conducted, and whole-brain functional connectivity matrices were computed using Pearson correlation coefficients. Connections with coefficients greater than 0.9 were defined as high-intensity links, representing activation states in each session [17], and visualized for two randomly selected participants (Fig. 7).

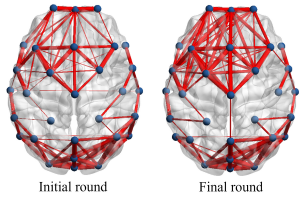

(a) Subject S01.

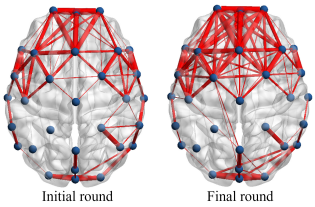

(b) Subject S03.

Fig. 7: Changes of high-intensity functional connectivity in trial-averaged EEG signals between the initial round and the final round within the immersive paradigm for two subjects.

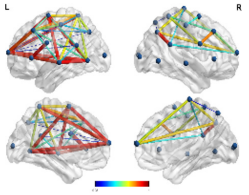

(a) Standard paradigm.

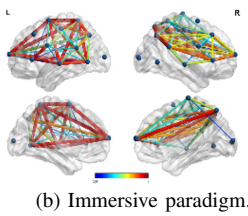

(b) Immersive paradigm.

Fig. 8: The status of effective whole-brain functional connectivity of the averaged EEG signals in the final round under the immersive and standard paradigms.

As illustrated in Fig. 7(a) and (b), both participants showed an increase in the number of high-intensity functional connections in the final round of the immersive paradigm compared to the initial round. Although spatial patterns varied individually, connections within the frontal, central, temporal, and occipital regions exhibited a consistent strengthening, indicating enhanced activation of cortices related to emotion regulation, motor control, auditory processing, and visual perception. These findings confirm the effectiveness of the immersive paradigm as an NFT-based approach for promoting stronger activation in targeted brain regions.

To further compare the immersive paradigm with the standard paradigm, averaged trial data from the final session of all participants were used to visualize whole-brain effective connections, defined as those exceeding a correlation strength of 0.7 (Fig. 8) [18].

In the standard paradigm, participants established an average of 71 effective connections, of which 42 were high-intensity, primarily concentrated in the frontal and occipital lobes (Fig. 8(a)). High-intensity links were more prevalent in the right hemisphere, while other regions exhibited comparatively fewer effective connections.

In contrast, under the immersive paradigm, participants formed an average of 101 effective connections, including 54 high-intensity ones, distributed across the prefrontal, temporal, central, occipital, and parietal regions (Fig. 8(b)). Notably, the right hemisphere showed stronger high-intensity connections between the prefrontal and parietal cortices, whereas the left hemisphere displayed denser connections spanning the frontal, temporal, and occipital areas.

Overall, the immersive paradigm established a larger number of stronger connections that engaged visual, auditory, emotion regulation-related, and motor cortices. These results demonstrate its superiority in promoting more extensive and effective functional connectivity across the brain.

IV. CONCLUSION

In summary, this study has introduced a multisensory neurofeedback-based immersive BCI paradigm built on the GRAIL platform, which has been designed to overcome the inherent limitations of conventional approaches. Comparative results with the standard paradigm have demonstrated that the proposed design, by integrating visual, auditory, and motor feedback, has achieved superior outcomes in multisensory coordination and cognitive–motor training. Furthermore, this paradigm has effectively enhanced the activation of brain regions involved in emotion regulation and facilitated the establishment of functional connectivity within these networks. Ultimately, it has promoted stronger engagement of emotion regulation-related areas, underscoring its potential to improve the efficiency of emotion regulation training in brain rehabilitation. Looking ahead, we plan to extend this BCI paradigm into an NFT game, aiming to achieve improved levels of immersion, participant engagement, and training effectiveness.

REFERENCES

[1] R. Sitaram, T. Ros, L. Stoeckel, S. Haller, F. Scharnowski, J. Lewis-Peacock, N. Weiskopf, M. Blefari, M. Rana, E. Oblak, N. Birbaumer, and J. Sulzer, "Closed-loop brain training: The science of neurofeedback," *Nature Reviews Neuroscience*, vol. 18, 12 2016.

[2] T. Nguyen, T. Zhou, T. Potter, L. Zou, and Y. Zhang, "The cortical network of emotion regulation: Insights from advanced eeg-fmri integration analysis," *IEEE transactions on medical imaging*, vol. 38, no. 10, pp. 2423–2433, 2019.

[3] W. Li, Y. Li, D. Cao, Z. Qian, Y. Tang, and J. Wang, "Tms-eeg signatures of facilitated cognitive reappraisal in emotion regulation by left ventrolateral prefrontal cortex stimulation," *Neuropsychologia*, vol. 184, p. 108560, 2023.

[4] A. U. Patil, C. Lin, S.-H. Lee, H.-W. Huang, S.-C. Wu, D. Madathil, and C.-M. Huang, "Review of eeg-based neurofeedback as a therapeutic intervention to treat depression," *Psychiatry Research: Neuroimaging*, vol. 329, p. 111591, 2023.

[5] A. Watve, A. Haugg, N. Frei, Y. Koush, D. Willinger, A. B. Bruehl, P. Stämpfli, F. Scharnowski, and R. Sladky, "Facing emotions: Real-time fmri-based neurofeedback using dynamic emotional faces to modulate amygdala activity," *Frontiers in Neuroscience*, vol. 17, p. 1286665, 2024.

[6] J. A. Pereira, A. Ray, M. Rana, C. Silva, C. Salinas, F. Zamorano, M. Irani, P. Opazo, R. Sitaram, and S. Ruiz, "A real-time fmri neurofeedback system for the clinical alleviation of depression with a subject-independent classification of brain states: A proof of principle study," *Frontiers in Human Neuroscience*, vol. 16, p. 933559, 2022.

[7] L. Castanho, D. V. Martinho, A. C. Saial, B. R. Gouveia, É. R. Gouveia, and F. Ribeiro, "The efficacy of virtual reality-based eeg neurofeedback in health-related symptoms relief: a systematic review," *Applied psychophysiology and biofeedback*, pp. 1–21, 2025.

[8] J. J. Gross, "Antecedent-and response-focused emotion regulation: divergent consequences for experience, expression, and physiology." *Journal of personality and social psychology*, vol. 74, no. 1, p. 224, 1998.

[9] P. Korzeniowski, S. Płotka, R. Brawura-Biskupski-Samaha, and A. Sitek, "Virtual reality simulator for fetoscopic spina bifida repair surgery," in *2022 IEEE/RSJ International Conference on Intelligent Robots and Systems (IROS)*. IEEE, 2022, pp. 401–406.

[10] E. T. Rolls, "The cingulate cortex and limbic systems for emotion, action, and memory," *Brain structure and function*, vol. 224, no. 9, pp. 3001–3018, 2019.

[11] V. Zotev, R. Phillips, H. Yuan, M. Misaki, and J. Bodurka, "Self-regulation of human brain activity using simultaneous real-time fmri and eeg neurofeedback," *NeuroImage*, vol. 85, pp. 985–995, 2014.

[12] L. Zhang, M. Lei, J. Zhang, Z. Huang, R. Huang, and H. Cheng, "Engaging mind and body: An immersive bci paradigm with motion-panoramic virtual reality," in *2025 IEEE/RSJ International Conference on Intelligent Robots and Systems (IROS)*. IEEE, 2025, pp. 13 103–13 110.

[13] L. Dickey, A. Dao, S. Pegg, and A. Kujawa, "Neural markers of emotion regulation difficulties in adolescent depression and risk for depression," *Journal of Mood & Anxiety Disorders*, vol. 5, p. 100051, 2024.

[14] B. H. Kim, J. Ho Kwak, M. Kim, and S. Jo, "Affect-driven robot behavior learning system using eeg signals for less negative feelings and more positive outcomes," in *2021 IEEE/RSJ International Conference on Intelligent Robots and Systems (IROS)*, 2021, pp. 4162–4167.

[15] Y. Si, F. Li, K. Duan, Q. Tao, C. Li, Z. Cao, Y. Zhang, B. Biswal, P. Li, D. Yao, and P. Xu, "Predicting individual decision-making responses based on single-trial eeg," *NeuroImage*, vol. 206, p. 116333, 2020.

[16] M. Xia, J. Wang, and Y. He, "Brainnet viewer: a network visualization tool for human brain connectomics," *PloS one*, vol. 8, no. 7, p. e68910, 2013.

[17] X. Xin, Z. Wang, S. Jia, S. Li, Q. Liu, X. Wang, and X. Wang, "Brain functional connectivity characteristics at various levels of inhibitory function in elderly individuals with cognitive impairment," *Scientific Reports*, vol. 15, no. 1, p. 27828, 2025.

[18] J. Chen, S. Wang, E. He, H. Wang, and L. Wang, "The architecture of functional brain network modulated by driving during adverse weather conditions," *Cognitive neurodynamics*, vol. 17, no. 2, pp. 547–553, 2023.